

Slow two-phase flow in artificial fractures: Experiments and simulations

Håkon Amundsen, Geri Wagner,¹ Unni Oxaal,² Paul Meakin, Jens Feder,
and Torstein Jøssang

Department of Physics, University of Oslo, Oslo, Norway

Abstract. The slow displacement of a wetting fluid by a nonwetting fluid in models of a single fracture was studied experimentally and by computer simulations on identical geometries. The fracture was modeled by the gap between a rough plate and a smooth transparent plate, both oriented horizontally. Two different rough plates were used, a textured glass plate and a polymethyl methacrylate plate with a computer-generated pattern. A nonwetting fluid (air) was injected slowly through an inlet into the model and displaced a wetting fluid (water) initially filling the model. The aperture fields of the artificial fractures were measured using a light absorption technique. The experiments were simulated using modified invasion percolation models, making use of the measured aperture fields. The simulation models captured invasion bursts and fragmentation and redistribution of the invading air. Experiments and simulations were compared step by step, and good qualitative and quantitative agreement was found.

1. Introduction

Fluid flow in fractured subsurface environments is of central interest to many geologic engineering applications, including groundwater protection, nuclear waste isolation and enhanced oil recovery. In rocks containing open fractures, fluids tend to flow in the fractures rather than in the rock matrices, since the matrices generally are much less permeable than the fractures. On the microscopic scale, single-phase flow through a single fracture has been studied experimentally by means of tracer injection and flow rate measurements. Theoretical calculations of flow in a single fracture usually involve a square lattice of sites in which random, spatially correlated apertures are assigned to the sites. In this approach, each site represents a region of the fracture with approximately constant aperture. By computing the fluid pressure at each node of the mesh, the steady state flow rates between all the nodes may be obtained.

If more than one fluid phase is able to flow, additional complexity is introduced due to the interactions between the fluid phases. Approximating a fracture by two parallel, smooth plates, several researchers [e.g., *Fourar et al.*, 1993; *Pan et al.*, 1998] studied the phase distributions in flow experiments. *Nicholl and Glass* [1994] measured relative permeabilities in steady state, two-phase flow through a transparent artificial fracture made of two textured glass plates. *Wan et al.* [1996] used etched glass micromodels to observe flow patterns and displacement processes in a fractured porous medium.

Experimental data involving two-phase flow in natural fractures are scarce owing to the considerable experimental difficulties involved. *Merill* [1975] and *Reitsma and Kueper* [1994]

studied two-phase flow through a natural rock fracture indirectly by pressure measurements in and across the fracture. *Nicholl et al.* [1994] opened an initially dry natural fracture after flooding with a wetting fluid to study the displacement pattern. *Pyra-Nolte et al.* [1992] and *Persoff and Preuss* [1995] used transparent replicas of a natural rock fracture to directly observe two-phase flow patterns.

A number of models have been proposed to simulate slow two-phase flow through a single fracture [*Wanfang et al.*, 1997]. These models are related to the general percolation problem and divide the void space of the fracture into regions that are occupied by one or the other of the two phases. *Pruess and Tsang* [1990] and *Pyra-Nolte et al.* [1990] used a square lattice of sites to represent a single fracture and to calculate steady state relative permeabilities. Each site with an aperture b less than a cutoff aperture was occupied by the wetting fluid, and the remaining sites were occupied with the nonwetting fluid. *Pyra-Nolte et al.* [1992] studied the invasion of a wetting fluid in a fracture filled with a nonwetting fluid and modeled the process using a percolation process in which the accessibility of different regions in the fracture was taken into account. *Mendoza and Sudicky* [1991] reported simulations using a similar fracture model. A displacement pattern was simulated using invasion percolation with trapping [*Wilkinson and Willemsen*, 1983] and the relative permeability of the model was computed as a function of saturation with the nonwetting fluid. *Glass* [1993] developed a modified invasion percolation model to simulate the imbibition of wetting fluids into fractures, under the influence of gravity. At each stage in the simulation, the local curvature of the fluid-fluid interface was used to define the invasion thresholds of sites on a square lattice. *Paterson et al.* [1996], *Du et al.* [1996], and *Wagner et al.* [1999] studied displacement patterns obtained from standard invasion percolation models on correlated substrates. These substrates had fractal properties and represented sections of strongly heterogeneous rocks, such as fractured rocks.

At present, it is not clear as to what degree percolation models capture real-world displacement processes in single

¹Now at Sackler Faculty of Exact Science, School of Astronomy and Physics, Tel Aviv University, Tel Aviv, Israel.

²Now at Department of Agricultural Engineering, Agricultural University of Norway, Aas.

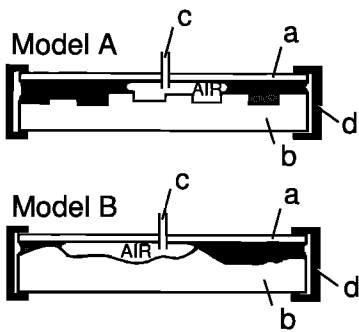


Figure 1. Schematic drawing of the two artificial fracture models A and B used in the experiments. Labeled are as follows: a, plane top plate; b, rough bottom plate; c, air inlet; and d, clamps.

fractures. In this paper we present, for the first time, a detailed comparison of experiments and simulations of slow, two-phase flow in fractures. We used artificial fracture models constructed from a rough horizontal bottom plate covered by a plane transparent top plate and filled with a wetting fluid (water). The aperture field of the first model was prepared with discrete values, to facilitate direct comparison of the displacement patterns with the simulation. The second model had a continuous aperture field that appeared to be a closer approximation to natural fracture geometries. In both models, water was slowly displaced by a nonwetting fluid (air), and the development of the fluid occupancy patterns was recorded.

The displacement processes were simulated using the void space geometries measured from the models. The simulations were based on the invasion percolation (IP) model [Lenormand and Bories, 1980; Wilkinson and Willemse, 1983]. In the IP model, random numbers ("invasion thresholds") are assigned to each site on a lattice representing a random medium. Initially, all but one of the sites are occupied by the wetting fluid ("defender fluid"), and one site is occupied by the nonwetting fluid ("invader fluid"). The algorithm then consists of repeating two steps:

1. Identify the defender fluid site adjacent to the invaded region that has the lowest invasion threshold.

2. Invade the identified site by filling it with invader fluid.

The IP model has proven to be very successful in describing the displacement of wetting fluids by a nonwetting fluids in porous media, in the case of vanishing viscous forces [Lenormand and Zarcone, 1985]. The success of the IP algorithm is due to the correspondence between the invasion thresholds assigned to the sites and the random capillary pressures P_c that the nonwetting fluid must overcome to invade a pore. For a circular pore of radius r , P_c is given by

$$P_c = \frac{2\sigma \cos \theta}{r}, \quad (1)$$

where σ is the interfacial tension and θ is the angle of contact with respect to the matrix material.

Capillary forces may also be expected to play a dominant role in two-phase flow through narrow fractures. The pressure that the nonwetting fluid must overcome to invade a region with aperture b is given by [Kueper and McWhorter, 1991]

$$P_c = \frac{2\sigma \cos \theta}{b}. \quad (2)$$

In contrast to the fluid-fluid interface in a porous medium, the fluid interface in a fracture is not divided into numerous menisci separated by a solid matrix but is continuous.

2. Experiments

The experiments were conducted using artificial fracture models in which (nonwetting) air displaced (wetting) water. This combination of fluids was characterized by the interfacial tension $\sigma = 0.072 \text{ N m}^{-1}$, and a viscosity ratio of $M = 2 \times 10^{-2}$. The air injection rate was kept low (1 mL min^{-1}) to minimize viscous forces. The fluid-fluid interface propagated with an average velocity of approximately $5 \times 10^{-5} \text{ m s}^{-1}$, corresponding to a low capillary number of $\text{Ca} = 1 \times 10^{-8}$.

Figure 1 shows the experimental setup. The models consisted of two plates of equal dimensions that were clamped together. The bottom plate was rough, whereas the top plate was smooth. A central hole drilled in the top plate provided an inlet for the air. Gravitational effects were minimized by orienting the model horizontally, and displaced water was collected at the boundary of the model.

Two different rough bottom plates were used with smooth planar top plates. The corresponding laboratory models (and computer models) are referred to as model A and model B. Both models had a mean aperture of approximately 0.15 mm. The bottom plate of model A was a 25-mm-thick polymethyl methacrylate (PMMA) plate in which a lattice of 40×40 square regions of different depths was milled. A Dekel milling machine with an accuracy of 1 μm was used. The mill was controlled by computer using a computer-generated model for the desired surface geometry. The size of each site was 5×5 mm, and the milling depth ranged from 0.0 mm to 0.30 mm in steps of 0.01 mm. The surface of the bottom plate was self-affine and was constructed to have a Hurst exponent of $H = 0.8$. The Hurst exponent is a measure for the roughness of a self-affine surface and varies from 0 to 1, with $H = 1$ characterizing a smooth surface.

In model B a textured 30 \times 30 cm glass plate was used as the bottom plate. The aperture variations in this model were continuous. The aperture field was measured employing a light absorption technique [Nicholl and Glass, 1994]. The model was filled with water containing 0.1 wt% Nigrosine dye and placed on a light box. In the resulting pattern of gray shades, dark patches indicated regions with large apertures, because the intensity of the transmitted light decreases with the distance traveled through the absorbing layer. Using a high-resolution (2000 \times 2000 pixels), cooled charge-coupled device (CCD) camera with 12-bit intensity resolution, a digital image of the model was analyzed and found to yield a consistent map of the relative order of the apertures. Transmission errors due to refraction effects at the fluid-solid interface were ignored, since the local slope of the model bottom plate was low everywhere. The apertures ranged from 0 to 0.35 mm and were approximately lognormally distributed.

In both models, top plates of the same material as the bottom plates were used to create uniform wetting conditions. The water used in the experiment was de-aerated to avoid the formation of air bubbles. The models were filled by pouring water onto the bottom plate until the plate was completely covered. At this stage the top plate was brought in place. Air was injected through the air inlet at a constant rate and penetrated into the fracture model. Images of the displacement pattern were recorded every 2 min using a Nikon 35-mm cam-

era. In some experiments, a sensitive pressure sensor and a PC were used to record the air pressure at the inlet at 1-s intervals. An experiment lasted until the air reached one of the edges of the model (breakthrough); this usually occurred after 30 min to 1 hour.

Figure 2 shows several stages in the growth of a displacement pattern from an experiment using model A. The lattice sites with constant apertures can be recognized as square regions with the same gray level. The essentially discrete gray levels in the figure correspond to the discrete apertures in the underlying numerical model. Figure 2 shows that the growth of the air cluster was correlated with the aperture field. The width of the “arms” stretching out from the central “body” of air (Figure 2a) was equal to the lattice constant of the model. Air generally invaded the regions with the largest aperture, as expected. At later stages (Figure 2b and 2c), more narrow regions were invaded as well, and the arms often widened out to two or three lattice constants. In Figure 2c, trapped islands of water may be observed.

Model A included 1600 sites and only 30 different aperture sizes. At some stages, several water-filled sites adjacent to the growing cluster of air had apertures of the same size. As a result of those degeneracies, the cluster of air did not grow in a completely reproducible manner in different experiments. At the degenerated stages, the outcome of the experiment was determined by impurities in the model or by inaccuracies of the model geometry that were due to slight deformation of the bottom plate.

Figure 3 shows a plot of the pressure at the air inlet (the capillary pressure P_c), plotted as a function of time. The pressure curve is correlated to the sequence of regions invaded by the cluster of air. During the first 6 min, the air pressure increased almost linearly, and only a small region near the injection point was invaded (Figure 2a). The pressure decreased rapidly as a large number of sites were invaded almost instantaneously (Figure 2b). Similarly, the other rapid pressure reductions may be identified with invasion bursts. This is confirmed by the plot of the number of invaded model sites, plotted as a function of time on the same graph. During these burst-like events viscous forces must become more important relative to the capillary forces. However, they do not play an important role in the pattern formation process because only wide aperture regions are invaded, and the patterns are controlled by the distribution of small-aperture regions. The pressure variations were reproducible and of the expected order of magnitude (≈ 1000 Pa), predicted by equation (2) with $\sigma = 0.072\text{N/m}$, $\theta = 0$, and a mean aperture of $\bar{b} = 0.15\text{ mm}$.

Figure 4 shows a time series from a displacement experiment carried out using model B. The aperture field in the model was anisotropic, with “valleys” of high aperture and “ridges” of low aperture in the east-west direction. As in model A, the developing displacement pattern was correlated with the aperture variations in the model, and the displacement process was episodic. In Figures 4b and 4c the results of “snap-off” events may be seen in which bubbles of air became isolated from the large air cluster connected to the inlet.

The air bubbles in model B were separated from each other by regions with relatively low apertures (the ridges) acting as barriers. The bubbles had a considerable “storage capacity,” reflected by advances and retractions of the fluid-fluid interfaces [Måløy *et al.*, 1992]. Fresh air could be transported over the ridges via a sequence of small bubbles. When the pressure in the cluster connected to the air inlet had increased suffi-

ciently, the cluster could connect to a neighboring bubble. The neighboring bubble was inflated and its interface pushed outward until contact was established with the next neighbor bubble. When air was transported through the connected chain of bubbles to a water-invaded region with a large aperture, the region was invaded, and the air chain fragmented (this fragmentation is called a snap-off). The timescale on which snap-offs and invasion bursts occurred was of the order of 1 s. Invasion bursts were separated by several minutes. In all experiments using model B, similar or identical displacement patterns were obtained. For technical reasons, no reproducible pressure measurements could be obtained with model B.

The displacement patterns observed in the two models differ in two respects: First, trapping of water occurred in model A but not in B; second, snap-off of invading air occurred in model B but not in A. Trapping may have been prevented in model B due to the pronounced “valleys” in the model. The air “pushed” the water along the valleys rather than encircled water-filled regions.

The absence of snap-offs in model A may be related both to the isotropy of the model and to the discrete aperture variations. In model A, the air occupied only sites with large apertures, whereas in model B the invading fluid was forced to pass over low-aperture ridges in order to pass from valley to valley. The pressure fluctuations accompanying the invasion of narrow sections could lead to snap-offs. Moreover, in model A the fluid-fluid interface was always located in regions with locally constant aperture (see Figure 1a). In model B the continuous aperture variations led to nonvanishing gradients in the capillary pressure and thus redistribution of the air.

3. Simulations

The displacement processes observed in model A were simulated using a variant of the standard IP model without trapping [Lenormand and Bories, 1980; Wilkinson and Willemsen, 1983]. The IP model is conceptually very simple, focusing on capillary forces only. It does not account for other, potentially important factors such as film flow of the wetting fluid along the fracture surface [Tokunaga and Wan, 1997]. In the present implementation, a square lattice of 40×40 sites was used, corresponding to the square regions of known (discrete) apertures forming the void space in the experimental model. The invasion threshold p_i of the i th site was given by the inverse of the aperture b_i in the i th region.

The simulation began by invading a site in the center of the lattice representing the air inlet. The cluster of invaded sites expanded as the IP algorithm outlined in section 1 was executed. Two different strategies may be used to account for the degenerate configurations mentioned in section 2: either simultaneous invasion of all sites with lowest threshold, or random selection of one of those sites. In this work, the simultaneous invasion strategy was used.

The snap-off events and redistribution of air observed in model B cannot be reproduced using the standard IP model. A modified IP model that included migration of invader fluid and fragmentation of the IP cluster was developed. As in standard IP, the simulation proceeded in steps and began by invading the injection site. After each invasion step, one or more migration steps in which the invader fluid was redistributed could take place. The migration mechanism modeled the transport of air through air bubbles observed in fracture model B. During migration, invader fluid from a site at the perimeter of a cluster

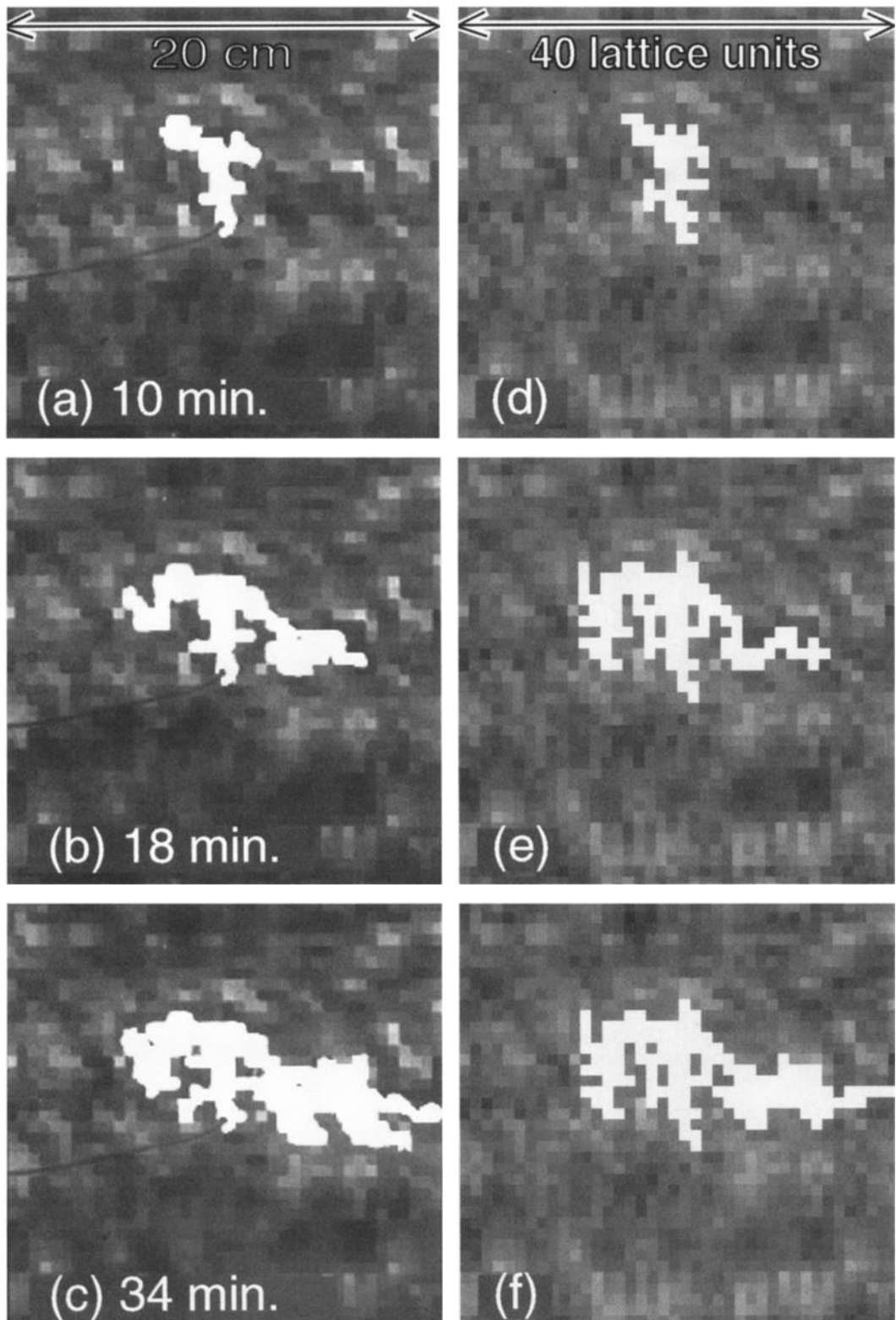


Figure 2. (left) Displacement patterns observed during an experiment using model A. Air (white) displaced wetting water (gray). The gray shades indicate the aperture of the model, with the darkest shades representing the largest apertures. The injection tube leading to the center of the model is visible. (right) Simulated displacement patterns using a modified IP model with simultaneous invasion on a lattice of 40×40 sites. The nonwetting fluid (white) displaces the wetting fluid (gray). The gray shades represent the invasion thresholds used, with the darkest shades representing the lowest thresholds.

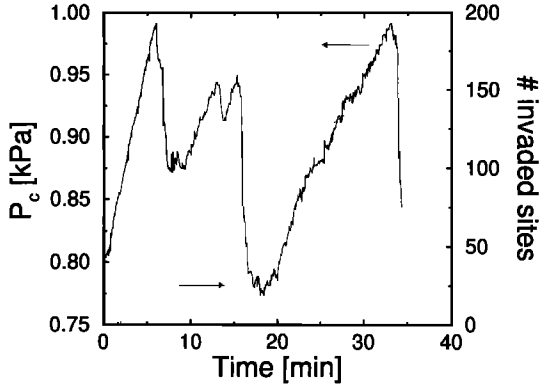


Figure 3. Plot of the air pressure at the inlet P_c as a function of time, measured in the experiment shown in Figure 2. On the same graph is shown a plot of the number of invaded model sites (right-hand scale; dotted line) as a function of time.

was withdrawn while an adjacent site was invaded (see Figure 5). A migration step was possible only if the aperture of the adjacent site was larger than that of the cluster site from which the air was withdrawn. Transfer of “fluid” always took place between the combination of sites that had the largest difference in aperture. All possible migration steps were carried out before a new invasion took place.

Migration steps could lead to fragmentation of a cluster. A cluster fragment could migrate on its own and coalesce with other fragments. Invasion was restricted to the cluster of sites that was connected to the injection site. Here a cluster of sites is defined as a set of sites with the same label (representing either wetting fluid or nonwetting fluid) in which every site is connected to all of the other sites by a path that consists of steps between nearest neighbor sites with the same label. A trapping rule was used during invasion steps and during migration steps to conserve the volume of entrapped water. This rule required that water-filled sites that were not connected to the lattice boundary by a path of nearest neighbor water-filled sites could not be invaded. Instead, the volume of disconnected “islands” of water was conserved.

In the simulations, the area covered by a migrating cluster (the number of sites belonging to the cluster) remained constant, whereas the volume occupied by the cluster (the sum of the apertures of the sites covered by the cluster, multiplied by the area of each site) varied. The migration steps modeled the cluster’s tendency to maximize its volume and to minimize its internal pressure. In contrast, in the experiments the area of the projection of a migrating bubble onto a horizontal plane varied. The volume and pressure changes experienced by a migrating bubble can be assumed to be small, since the capillary pressure variations experienced by the bubble were small compared with atmospheric pressure. By construction, the simulation model thus exaggerates the volume changes of the bubble and ignores the change in projected area of the bubble.

The simulation of the displacement process in the fracture model B was carried out using a square lattice of 230×230 sites. The invasion thresholds assigned to the sites were obtained by coarse-graining the aperture field measured in model B. The threshold of the i th site was equal to the inverse of the mean aperture of the region represented by the site.

4. Comparison of Experiments and Simulation

To compare the experiments with the simulations, the experimental displacement patterns were divided into sections corresponding to the lattice sites used in the simulations, and a site-by-site comparison scheme was applied. The overlap S between an experimental pattern and a simulated pattern, with N_E and N_S air-filled sections, respectively, was defined as

$$S = N_0/N, \quad (3)$$

where N_0 is the number of air-filled sections in the experimental pattern and the simulated pattern that overlapped each other, and $N = \min(N_E, N_S)$. Since pictures were taken at equal intervals during an experiment and invasion occurred in bursts, and since the simultaneous invasion scheme was used in the simulations, an exact match of N_E and N_S was not always obtainable. Those stages in the experiments and simulations that had the least difference $|N_E - N_S|$ were compared. To find N_0 and N , photographs of the experimental patterns were digitized and the air-filled regions were identified. A 40×40 square grid was placed on the photographs from experiments on model A, and the sections that were more than 50% invaded by air were marked manually. The photographs from the experiments on model B were divided into a square grid of the same size as the one used in the simulations, and image-processing software was used to identify the sections that were invaded by air.

Figure 6 illustrates the overlap between the displacement patterns observed in model A and that obtained from the standard IP model with simultaneous invasion. Similarly, Figure 7 illustrates the overlap between the patterns observed in model B and that obtained from the modified IP model with fluid redistribution. A plot of the overlap S as a function of the size of the smaller of the two clusters N for four different experiments using model A and the standard IP model with simultaneous invasion is shown in Figure 8. The general agreement is good, with more than 70% overlap during most of the displacement. The poor overlap around $N = 100$ is due to the delayed invasion of a large region to the east of the injection site in the simulation.

Perfect overlap between the experiment and simulations should not be expected, since the experimental displacement pattern is affected by fluctuations in the wetting characteristics and inaccuracies of the experimental fracture model, as mentioned in section 2. In fact, at some stages the experimental cluster of air invaded water-filled regions at its perimeter that had, nominally, a slightly lower aperture than other perimeter regions, which were invaded subsequently. Fluctuations in the wetting characteristics can occur as a consequence of contamination of the surfaces and/or variations in the microscopic roughness of the surfaces.

Even in the absence of a trapping rule conserving the volume of water “islands,” the shape and the location of water-filled regions that were trapped by the air cluster was well reproduced. The apertures of these regions were small, and the regions were not invaded at any stage. In general, IP clusters grown on a self-affine substrate in the absence of a trapping rule are quite different from clusters grown in the presence of a trapping rule [Wagner et al., 1997].

A similar plot for the experiment and simulation with model B is shown in Figure 9. The agreement between experiment and simulation is surprisingly good, with S better than 80% during most of the displacement. The good agreement may be

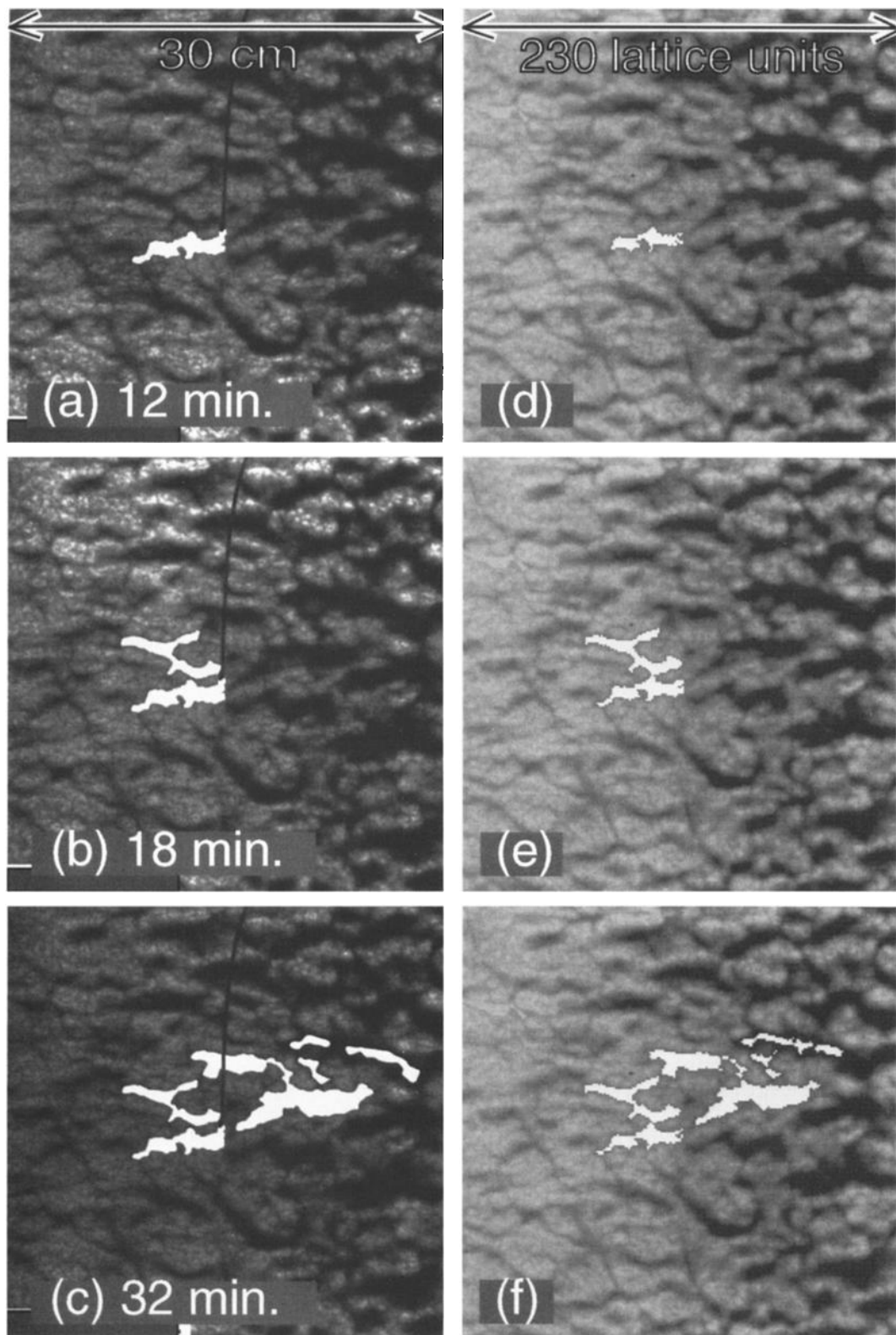


Figure 4. (left) Displacement patterns observed during an experiment using model B. Air (white) displaced wetting water (gray). The gray shades indicate the aperture of the model, with the darkest shades representing the largest apertures. The injection tube leading to the center of the model is visible. (right) Simulated displacement patterns using a modified IP model with fluid redistribution on a lattice of 230×230 sites. The nonwetting fluid (white) displaces the wetting fluid (gray). The gray shades represent the invasion thresholds used, with the darkest shades representing the lowest thresholds.

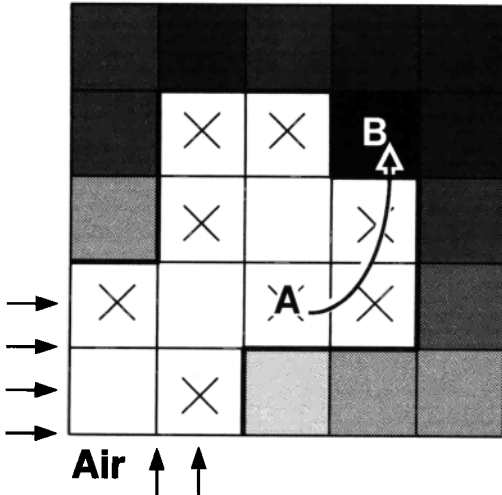


Figure 5. Illustration of the modified IP model used to simulate displacement in fracture model B. Shaded sites indicate water-filled regions, with dark shades indicating large apertures. “Air” was injected at the lower left corner and filled a region (white). In a migration step the perimeter site (crosses) with the smallest aperture (A) is filled with “water,” and the adjacent water-filled site with the largest aperture (B) is filled with air. The step is possible only if the aperture at B is larger than the aperture at A.

related to the fact that the aperture field was continuous and thus no aperture degeneracies were present, as in model A. The modified IP model reproduces the disconnection of bubbles and positions the bubbles correctly, as is shown in Figure 7. The trapping rule used in the simulations of the displacements in fracture model B was seldom invoked, in agreement with the experimental observations (see section 2).

5. Summary

The aperture field in fracture model A was constructed with self-affine fractal scaling properties leading to long-ranged spatial correlations, in agreement with various recent studies of rock fracture geometries [e.g., *Power and Tullis*, 1991; *Schmittbuhl et al.*, 1993, 1995; *Odling*, 1994; *Brown*, 1995]. However, the model was limited in size (range of length scales) owing to

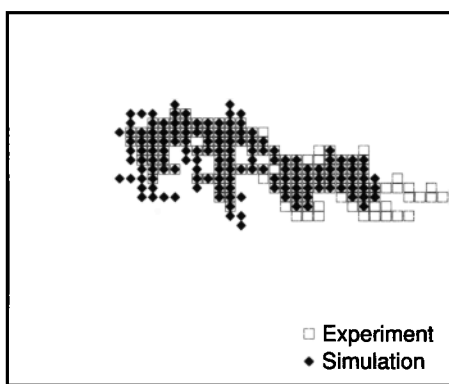


Figure 6. Comparison between the experimental pattern shown in Figure 2c and a simulated pattern obtained from the standard IP model with simultaneous invasion.

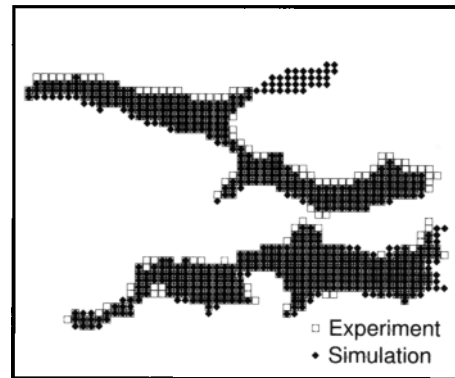


Figure 7. Comparison between the pattern of air-filled regions shown in Figure 4b and the simulated pattern obtained from the modified IP model with fluid redistribution.

technical constraints, and the effect of the discrete aperture variations is difficult to assess.

In model B the aperture variations were continuous as in a natural fracture. The aperture field in model B was found to have self-affine properties on length scales less than the typical width of the valleys (~ 20 mm). On these short scales the aperture field was characterized by a Hurst exponent $H = 0.82 \pm 0.08$. Above this length scale the aperture profile was dominated by the irregular valleys and ridges.

The standard IP algorithm with simultaneous invasion could not reproduce the displacement patterns observed in model B, since it does not include fragmentation mechanisms. On the other hand, the modified IP model with fluid redistribution had a poor ability to reproduce the experimental observations made using model A. The modified IP model predicted snap-offs to occur in model A, in contrast to the experimental observations. Similarly, in simulations of displacement in model B, snap-off was predicted to occur more often than was observed in the experiment. This weakness of the simulation model may possibly be corrected by taking into account the extra surface energy required to fragment a bubble of air. Low or high “cost factors” imposed on migration steps leading to fragmentation might favor or inhibit cluster formation, respectively. In fact, snap-off in model A was observed when the

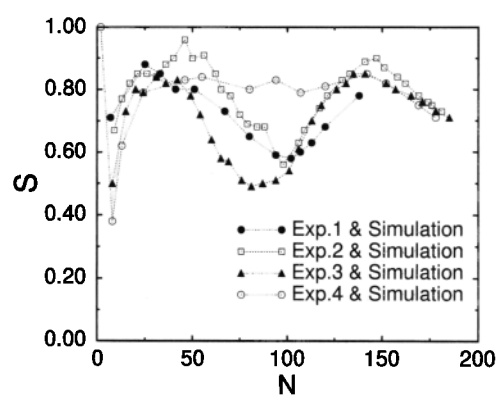


Figure 8. Plot of the overlap S between four different displacement experiments using model A and a simulation using the standard IP model with simultaneous invasion, as a function of the number of invaded sites, N .

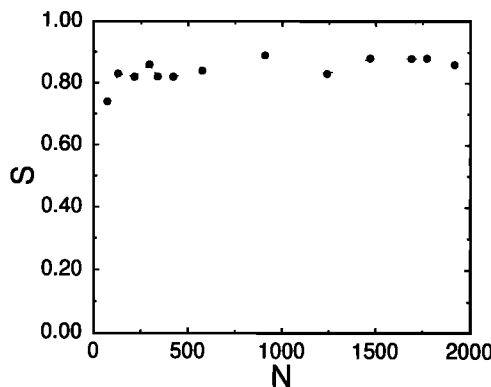


Figure 9. Plot of the overlap S between an experiment using model B and a simulation using the modified IP model with fluid redistribution, as a function of the number of invaded sites, N .

interfacial tension σ was decreased by adding soap to the water.

In conclusion, the slow displacement of water by air was studied experimentally using two different fracture models. The displacement processes were simulated using modified invasion percolation models, and the quality of the simulations was assessed by comparing the overlap between the experimental and the simulated displacement patterns.

The work reduces the gap between experimental studies of two-phase flow in fractures and numerical modeling of flow in fractures. Invasion percolation was found to describe slow, immiscible displacement processes in narrow fracture models quite well and led to accurate predictions of phase distribution in the models. However, the development of a single model that can simulate the displacement of a wetting by a nonwetting fluid in both types of fracture apertures remains a challenge for the future.

Acknowledgments. We gratefully acknowledge support by VISTA, a research cooperation between the Norwegian Academy of Science and Letters and Den Norske Stats Oljeselskap A.S. (STATOIL) and by NFR, the Norwegian Research Council. The work presented has received support from NFR through a grant of computing time.

References

- Brown, S. R., Simple mathematical model of a rough fracture, *J. Geophys. Res.*, 100(B4), 5941–5952, 1995.
- Du, C., C. Satik, and Y. C. Yortsos, Percolation in a fractional Brownian motion lattice, *AIChE J.*, 42(8), 2392–2395, 1996.
- Fourar, M., S. Bories, R. Lenormand, and P. Persoff, Two-phase flow in smooth and rough fractures: Measurement and correlation by porous-medium and pipe flow models, *Water Resour. Res.*, 29(11), 3699–3708, 1993.
- Glass, R. J., Modeling gravity-driven fingering in rough-walled fractures using modified percolation theory, paper presented at 4th Annual International Conference on High Level Radioactive Waste Management, Las Vegas, Nev., April 26–30, 1993.
- Kueper, B. H., and D. B. McWhorter, The behavior of dense, non-aqueous phase liquids in fractured rock and clay, *Ground Water*, 29(5), 716–728, 1991.
- Lenormand, R., and S. Bories, Description d'un mécanisme de connexion de liaison destiné à l'étude du drainage avec piégeage en milieu poreux, *C.R. Acad. Sci. Paris*, 291, 279–283, 1980.
- Lenormand, R., and C. Zarcone, Invasion percolation in an etched network: Measurement of a fractal dimension, *Phys. Rev. Lett.*, 54(20), 2226–2229, 1985.
- Måløy, K. J., L. Furuberg, J. Feder, and T. Jøssang, Dynamics of slow drainage in porous media, *Phys. Rev. Lett.*, 68(14), 2161–2164, 1992.
- Mendoza, C. A., and E. A. Sudicky, Hierarchical scaling of constitutive relationships controlling multi-phase flow in fractured geologic media, in *Reservoir Characterization: 3rd International Technical Conference: Papers*, edited by B. Linville, pp. 505–514, Pennwell, Tulsa, Okla., 1991.
- Merill, J. R. J., Two-Phase Flow in Fractures, Ph.D. thesis, Coll. of Eng., Univ. of Denver, Denver, Colo., 1975.
- Nicholl, M. J., and R. J. Glass, Wetting phase permeability in a partially saturated horizontal fracture, in *High-Level Radioactive Waste Management*, pp. 2007–2019, Am. Nucl. Soc., La Grange Park, Ill., 1994.
- Nicholl, M. J., R. J. Glass, and S. W. Wheatcraft, Gravity-driven infiltration instability in initially dry nonhorizontal fractures, *Water Resour. Res.*, 30(9), 2533–2546, 1994.
- Odling, N. E., Natural fracture profiles, fractal dimension and joint roughness coefficients, *Rock Mech. Rock Eng.*, 27(3), 135–153, 1994.
- Pan, X., R. C. Wong, and B. B. Maini, Steady state immiscible oil and water flow in a smooth-walled fracture, *J. Can. Pet. Technol.*, 37(5), 52–59, 1998.
- Paterson, L., S. Painter, M. A. Knackstedt, and W. V. Pinczewski, Patterns of fluid flow in naturally heterogeneous rocks, *Physica A*, 235, 619–628, 1996.
- Persoff, P., and K. Pruess, Two-phase flow visualization and relative permeability measurement in natural rough-walled fractures, *Water Resour. Res.*, 31(5), 1175–1186, 1995.
- Power, W. L., and T. E. Tullis, Euclidean and fractal models for the description of rock surface roughness, *J. Geophys. Res.*, 96(B1), 415–424, 1991.
- Pruess, K., and Y. W. Tsang, On two-phase relative permeability and capillary pressure of rough-walled rock fractures, *Water Resour. Res.*, 26(9), 1915–1926, 1990.
- Pyrak-Nolte, L. J., D. D. Nolte, L. R. Myer, and N. G. W. Cook, Fluid flow through single fractures, in *Rock Joints*, edited by C. C. Barton and O. Stephansson, pp. 405–412, A. A. Balkema, Brookfield, Vt., 1990.
- Pyrak-Nolte, L. J., D. Helgeson, and G. M. Haley, Immiscible fluid flow in a fracture, in *Rock Mechanics*, edited by J. R. Tillerson and W. R. Wawersik, pp. 571–578, A. A. Balkema, Brookfield, Vt., 1992.
- Reitsma, S., and B. H. Kueper, Laboratory measurement of capillary pressure-saturation relationships in a rock fracture, *Water Resour. Res.*, 30(4), 865–878, 1994.
- Schmittbuhl, J., S. Gentier, and S. Roux, Field measurements of the roughness of fault surfaces, *Geophys. Res. Lett.*, 20(8), 639–641, 1993.
- Schmittbuhl, J., F. Schmitt, and C. Scholz, Scaling invariance of crack surfaces, *J. Geophys. Res.*, 100(B4), 5953–5973, 1995.
- Tokunaga, T., and J. Wan, Water film flow along fracture surfaces of porous rock, *Water Resour. Res.*, 33(6), 1287–1295, 1997.
- Wagner, G., P. Meakin, J. Feder, and T. Jøssang, Invasion percolation on self-affine topographies, *Phys. Rev. E*, 55(2), 1698–1703, 1997.
- Wagner, G., P. Meakin, J. Feder, and T. Jøssang, Invasion percolation in fractal fractures, *Physica A*, 264, 321–337, 1999.
- Wan, J., T. K. Tokunaga, C.-F. Tsang, and G. S. Bodvarsson, Improved glass micromodel methods for studies of flow and transport in fractured porous media, *Water Resour. Res.*, 32(7), 1955–1964, 1996.
- Wanfang, Z., H. S. Wheater, and P. M. Johnston, State of the art of modelling two-phase flow in fractured rock, *Environ. Geol.*, 31(3/4), 157–165, 1997.
- Wilkinson, D., and J. F. Willemsen, Invasion percolation: A new form of percolation theory, *J. Phys. A Math. Gen.*, 16, 3365–3376, 1983.
- H. Amundsen, J. Feder, T. Jøssang, P. Meakin, and U. Oxaal, Department of Physics, University of Oslo, Box 1048, Blindern, N-0316 Oslo 3, Norway.
- G. Wagner, Sackler Faculty of Exact Science, School of Astronomy and Physics, Tel Aviv University, 69978 Tel Aviv, Israel. (wagner@fractal.tau.ac.il)

(Received August 21, 1998; revised May 3, 1999; accepted May 5, 1999.)